Macromolecules

Article

Cite This: Macromolecules 2019, 52, 9476−9483

pubs.acs.org/Macromolecules

Morphology Control of Liposome - RAFT Oligomer Precursors to Complex Polymer Nanostructures

Mohammad-Amin Moradi,*[,†] Sam Tempelaar,[†] Alexander M. van Herk,[‡] and Johan P. A. Heuts*[,†]

[†]Department of Chemical Engineering and Chemistry & Institute for Complex Molecular Systems, Eindhoven University of Technology, P. O. Box 513, 5600 MB Eindhoven, The Netherlands

[‡]Institute of Chemical and Engineering Sciences, 1 Pesek Road, Jurong Island 627833, Singapore

Supporting Information

ABSTRACT: Different types of butyl acrylate (BA)-*co*-acrylic acid (AA) oligomers were synthesized via reversible addition-fragmentation chain transfer (RAFT) polymerization and mixed with extruded 200 nm dimethyldioctadecylammonium bromide vesicles. The resulting precursor structures form the basis for subsequent vesicle-templated polymerizations. Systematic variations in temperature, pH, oligomer length, and oligomer composition and their effects on precursor morphology were studied. Surprisingly, different morphologies were obtained, including capsules, protruded capsules, solid spheres, and multicompartment structures. For example, capsules and multicompartment structures were found to result from higher AA contents, and protruded capsules and solid particles resulted from lower AA contents. Subsequent chain extension of the RAFT oligomers resulted in polymer nanostructures resembling the precursor morphologies.

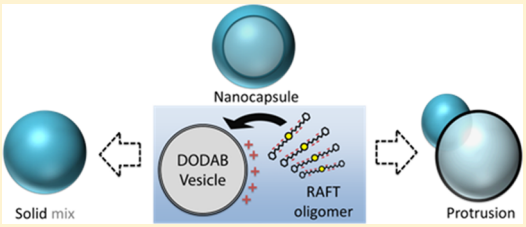

INTRODUCTION

As a type of soft templating, amphiphilic copolymers facilitate the synthesis of porous materials or hollow nanostructures.[1,2] The possible different morphologies, such as spherical, cylindrical, and bicontinuous phases of block copolymers, have provided controlled size and shape of the pores in materials like silica and carbon.[3] Additionally, scientists have used amphiphilic copolymers to prepare nanocapsules in a layer-by-layer approach, each layer building upon the previous layer with an opposite charge.[4−6] In an alternative approach, Ali et al. used a vesicle template and polymerized from the surface. The first step in that procedure involves the electrostatic interaction between the vesicle surface and an oppositely charged reactive oligomer, but rather than using layer-by-layer amphiphilic polymer additions in subsequent steps, the polymer shell was directly grown from the reactive oligomer.[7] The reactive, amphiphilic oligomer was synthesized by reversible addition-fragmentation chain transfer (RAFT) polymerization and thus contained a reactive end-group capable of chain extension. This so-called RAFT oligomer contained hydrophobic butyl acrylate (BA) and hydrophilic, anionic acrylic acid (AA) units, which could "attach" to the cationic dimethyldioctadecylammonium bromide (DODAB) vesicle surface. These RAFT oligomers were then chain-extended to achieve the desired shell thickness.[7−12] This process was found to result in several different final morphologies, including capsules, protruded capsules, parachute-like, and necklace-like structures.[13−16] In previous work, where we studied the effect of cross-linking during the chain extension step, we found that a significant part of the capsules showed protrusions, with about 20% of the capsules showing a protrusion when we did not use any cross-linker.[11] This result suggested that the final morphology may actually be "predefined" by the morphology of the oligomer-vesicle precursors, and the fact that the oligomers have a molar mass and chemical composition distribution makes it very conceivable that indeed different morphologies of the oligomer-vesicle precursors exist.[11]

In this paper, we investigate whether the precursors of the different structures can already be observed before the chain extension. We used a 2^{5-1} half-factorial experimental design[17] to systematically study the effects of different parameters in the precursor preparation (ratios of the vesicle to RAFT oligomer, pH, temperature, oligomer composition, and length) as they may have effects on the vesicle-oligomer precursor morphology and stability (see Scheme 1).[18−21]

EXPERIMENTAL SECTION

Experimental Design. The preparation of the oligomer-vesicle precursors consists of the adsorption of RAFT oligomers on the surface of DODAB vesicles by adding a vesicle solution to a stirred solution of the RAFT oligomers at a given temperature. Here, we investigate the effects of a range of parameters in this process on the resulting morphology using a 2^{5-1} half-factorial design, for which the factors and their levels are defined in Table 1. The levels are based on typical variations from our previous studies.[7,11]

Materials. Acrylic acid (AA, Fluka 99%), butyl acrylate (BA, Aldrich, 99%), Triton X-100 (TX-100, Sigma-Aldrich, 99%), dimethyldioctadecylammonium bromide (DODAB, Acros, greater

Received: October 15, 2019
Revised: November 26, 2019
Published: December 11, 2019

DOI: 10.1021/acs.macromol.9b02182
Macromolecules 2019, 52, 9476−9483

Scheme 1. Effect of Main Parameters on the Morphology of the Amphiphilic Polymer-Vesicle Structures

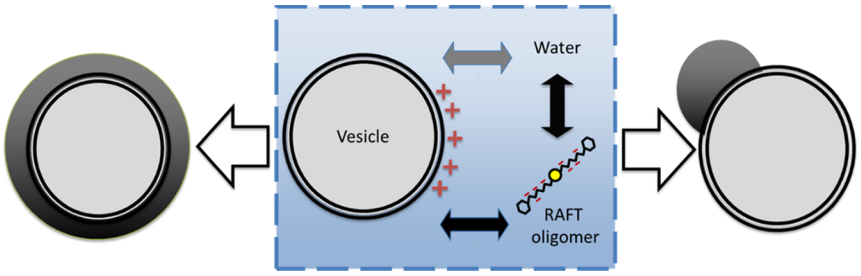

Table 1. Parameters and Ranges of the Designed Experiments

factor	low (−1)	high (1)
oligomer length (L)	18−22 units	28−31 units
temperature (T)	ambient	70 °C
pH	6	8
AA/DODAB ratio (R)	7.5	10
AA content in oligomer (F_{AA})	0.66	0.75

than 99%), methyl methacrylate (MMA, Aldrich, 99%), *tert*-butyl acrylate (*t*-BA, Aldrich, 98%), and ethylene glycol diacrylate (EGDA, Sigma-Aldrich, 98%) were used after inhibitor removal. Dioxane (Merck) and dimethyl sulfoxide-d_6 (Campro Scientific) were used as received. Distilled deionized (DDI) water was used throughout experiments. The RAFT agent dibenzyl trithiocarbonate (DBTTC, 99%) was synthesized as described before,[8] the initiator *N*,*N*′-azobis(isobutyronitrile) (AIBN, Fluka, 98%) was recrystallized from methanol, and the water-soluble azo initiator 4,4′-azobis-4-cyanovaleric acid (V-501, Fluka, 98%) was used as received.

Synthesis and Analysis of RAFT Oligomers. Four different RAFT oligomers were synthesized corresponding to the four possible combinations of length (L) and AA content (F_{AA}). The synthetic procedure of these oligomers has been described before,[10] and as an example, we describe here the synthesis of BA_6-*co*-AA_{12}. A monomer mixture of 11.9 g (0.093 mol) of BA and 13.4 g (0.192 mol) of AA was dissolved in 25 mL of dioxane and purged with argon before being added to a 100 mL three-neck flask containing a magnetic stirrer bar. To this mixture, 4.1 g (0.015 mol) of the RAFT agent DBTTC and 0.21 g (1.2×10^{-3} mol) of the initiator AIBN were added, and the polymerization was performed in a batch reaction for 5 h at 70 °C. Molar mass distributions (MWD), number-average molar masses (M_n), and the dispersities ($Đ$) of the RAFT co-oligomers were measured by size-exclusion chromatography (SEC), using a Waters SEC equipped with a Waters model 510 pump and a model 410 differential refractometer. Tetrahydrofuran was used as the eluent in two mixed bed columns (Mixed-C, Polymer Laboratories, 30 cm, 40 °C), and the system was calibrated using polystyrene standards (range = 580−7.5×10^6 g/mol). The average composition and degree of polymerization were determined via ^{1}H NMR spectroscopy on a Varian 400 MHz spectrometer (Figure S1), using dimethyl sulfoxide-d_6 as the solvent. The characteristics of the four oligomers are shown in Table 2.

Table 2. Molecular Characteristics of the RAFT Oligomers

	SEC		NMR	
oligomer	$Đ$	$M_{n,SEC}$ (g/mol)	$M_{n,NMR}$ (g/mol)	DP
BA_6-*co*-AA_{12}	1.23	14×10^2	1959	18
BA_5-*co*-AA_{17}	1.10	9×10^2	2123	22
BA_{10}-*co*-AA_{18}	1.14	16×10^2	2869	28
BA_7-*co*-AA_{24}	n.d.[a]	n.d.[a]	2847	31

[a]Not possible to determine by SEC.

Preparation of RAFT-Vesicle Nanostructures. A vesicle stock solution (A) was prepared by adding 0.652 g (1.03 mmol) of DODAB to 100 mL of DDI water and processed as explained earlier ($D_z \approx 200$ nm, $\zeta = +50$ mV).[8] A RAFT-copolymer solution (B) was prepared by adding BA_x-*co*-AA_y (see Table 2) to DDI water kept at pH = 7.5 using potassium hydroxide. Finally, a RAFT-vesicle dispersion (C) was then produced by addition of vesicle stock solution A into RAFT-oligomer solution B. The amounts of RAFT co-oligomer and vesicles are chosen in such a way that the ratio is kept at 2.5 (mol RAFT/mol DODAB) and is sufficiently far removed from the isoelectric point to avoid agglomeration as described in our previous study.[8] The particle size distribution and ζ potential of the RAFT-vesicle dispersion C were determined at 20 °C by dynamic light scattering (DLS), using a Malvern Zetasizer Nano ZS instrument. See the Supporting Information for details of the measurements.

Nanostructure Stability via Surfactant Lysis. The surfactant lysis experiments were done by adding Triton-X-100 solutions to the oligomer-vesicle mixtures (dropwise or by slow injection) as described in a reference.[12]

Cryo-TEM Morphology Characterization. Cryo-TEM was used under the standard conditions of using a type 3 Vitrobot to prepare a 3 μL sample blotted and plunged immediately into liquid ethane. The LaB_6 electron gun equipped Tecnai 20 microscope was set at 200 KV while imaging at −176 °C. Particle structures were distinguished based on their 2D projection and categorized in four groups:

(1) Solid particles with adsorbed RAFT oligomers (Figure 1A,B).

(2) Round hollow capsules (mostly appearing as circular structures in the 2D projection) with uniform shells (Figure 1C,D). This case includes the original vesicles.

(3) Protruded hollow structures of a RAFT-oligomer protrusion attached to a hollow structure resembling the previously described parachute-like structures[15] (Figure 1E,F).

(4) Multicompartment RAFT-vesicle structures observed as merged vesicles or onion-like structures (Figure 1G,H).

Several cryo-TEM images of each RAFT oligomer-DODAB vesicle mixture were taken in order to provide a representative number of particles under repeatable cryogenic sampling conditions. Particles have been counted and categorized in the relevant groups, and a frequency graph was made as described in our previous work.[11]

Polymerization from the Oligomer-Vesicle Precursor. Freshly prepared RAFT-vesicle dispersion C (17.5 mL) was transferred into a 50 mL three-neck flask equipped with a magnetic stirrer bar and a heating bath and diluted with 8 mL of DDI water. The reaction mixture was then purged with argon for 30 min at 70 °C under continuous stirring at 250 rpm. After addition of 7 mg (2.5×10^{-5} mol) of V-501 initiator, nanocapsules were synthesized by starved-feed emulsion copolymerization of MMA and BA (91 mol % MMA) using zero or 5% EGDA cross-linker.[11]

RESULTS AND DISCUSSION

The effect of the different factors listed in Table 1 on the morphology of the resulting oligomer-vesicle precursor was studied via a 2^{5-1} half-factorial experimental design, for which the parameter combinations are shown in Table 3. The dominant morphologies obtained in these different experiments are shown in Figure 2, and the fractions of the four

DOI: 10.1021/acs.macromol.9b02182
Macromolecules 2019, 52, 9476−9483

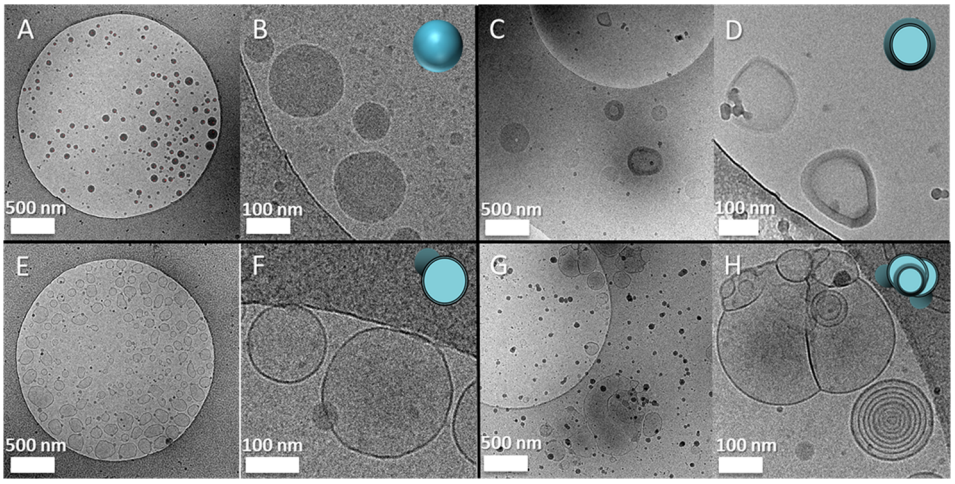

Figure 1. Different types of nanostructures prepared by the adsorption of random BA_x-AA_y RAFT oligomers onto DODAB vesicles: (A,B) solid spheres, (C,D) homogeneous capsules, (E,F) protruded hollow structures, and (G,H) multicompartment structures or onion-like structures.

Table 3. Summary of Experimental Design and Obtained Results[a]

exp.	L^1_{-1}	T^1_{-1}	pH^1_{-1}	R^1_{-1}	$F_{AA}{}^1_{-1}$	Y	Y_s	Y_c	Y_p	Y_m
1	−1	−1	−1	−1	1	100	2	95	1	2
2	1	−1	−1	−1	−1	99	100	0	0	0
3	−1	1	−1	−1	−1	10	100	0	0	0
4	1	1	−1	−1	1	0	8	61	12	19
5	−1	−1	1	−1	−1	100	0	13	87	0
6	1	−1	1	−1	1	99	7	56	0	37
7	−1	1	1	−1	1	100	3	91	0	6
8	1	1	1	−1	−1	96	2	3	73	21
9	−1	−1	−1	1	−1	100	100	0	0	0
10	1	−1	−1	1	1	98	0	77	20	3
11	−1	1	−1	1	1	9	0	97	2	1
12	1	1	−1	1	−1	0	22	12	22	49
13	−1	−1	1	1	1	100	0	100	0	0
14	1	−1	1	1	−1	99	0	18	65	7
15	−1	1	1	1	−1	12	0	19	81	0
16	1	1	1	1	1	0	1	30	5	64

[a] L (oligomer length), T (mixing temperature), pH (mixing pH), R (AA/DODAB ratio), and F_{AA} (AA fraction in the oligomer), all in coded units; Y (stable peak proportion after surfactant lysis, see the Supporting Information), Y_s (fraction of solid particles), Y_c (fraction of capsules), Y_p (fraction of protrusion structures), and Y_m (multicompartment structures) seen by cryo-TEM.

different morphology types observed in the overall population are summarized in Table 3: Y_s is the fraction of solid particles, Y_c is the fraction of homogeneous spherical capsules, Y_p is the fraction of protrusion structures, and Y_m is the fraction of multicompartment structures. The stability of the precursors to surfactant lysis is also shown as the response Y, which is the fraction of particles that survived the lysis experiments. Statistical analysis of these data was performed using the software package MINITAB,[22] and the results are shown in the Supporting Information.

When considering the data in Table 3, the first thing one notices is the fact that most samples are stable against TX-100 addition. This was an unexpected result because the same test was used previously to determine whether stable capsules were produced after chain extension.[12] Furthermore, capsule structures are present in most of the experiments and protrusions in about half of the experiments, with the greatest occurrence of protrusions in experiments using an oligomer with a low AA content (those with F_{AA} = 0.66 or in coded units: $F_{AA}{}^1_{-1}$= −1).

Multicompartment structures appear when nearly all factors are at the high level, but they are rarely the dominant structure in any of the experiments. In what follows, we describe the observed dependencies of the obtained morphologies on the preparation parameters in more quantitative detail.

Stability of Oligomer-Vesicle Precursors. The stability (Y) was quantified through the remaining proportion of the particles at the original size after TX-100 addition and is strongly dependent on the temperature at which the test is performed. Above their T_m, vesicles cannot withstand the presence of TX-100[8,12] even when decorated with the RAFT oligomers. Statistical analysis of the results in Table 3 (see the Supporting Information) results in the following relationship between the stability and the significant factors in coded units:

$$Y = 63.9 - 35.5\,T^1_{-1} + 11.9\,pH^1_{-1} + 11.8\,T^1_{-1}pH^1_{-1} \quad (1)$$

Equation 1 shows that low temperatures lead to stable precursor structures, regardless of the oligomer composition in the system and that a high temperature and low pH lead to a decreased stability.

DOI: 10.1021/acs.macromol.9b02182
Macromolecules 2019, 52, 9476−9483

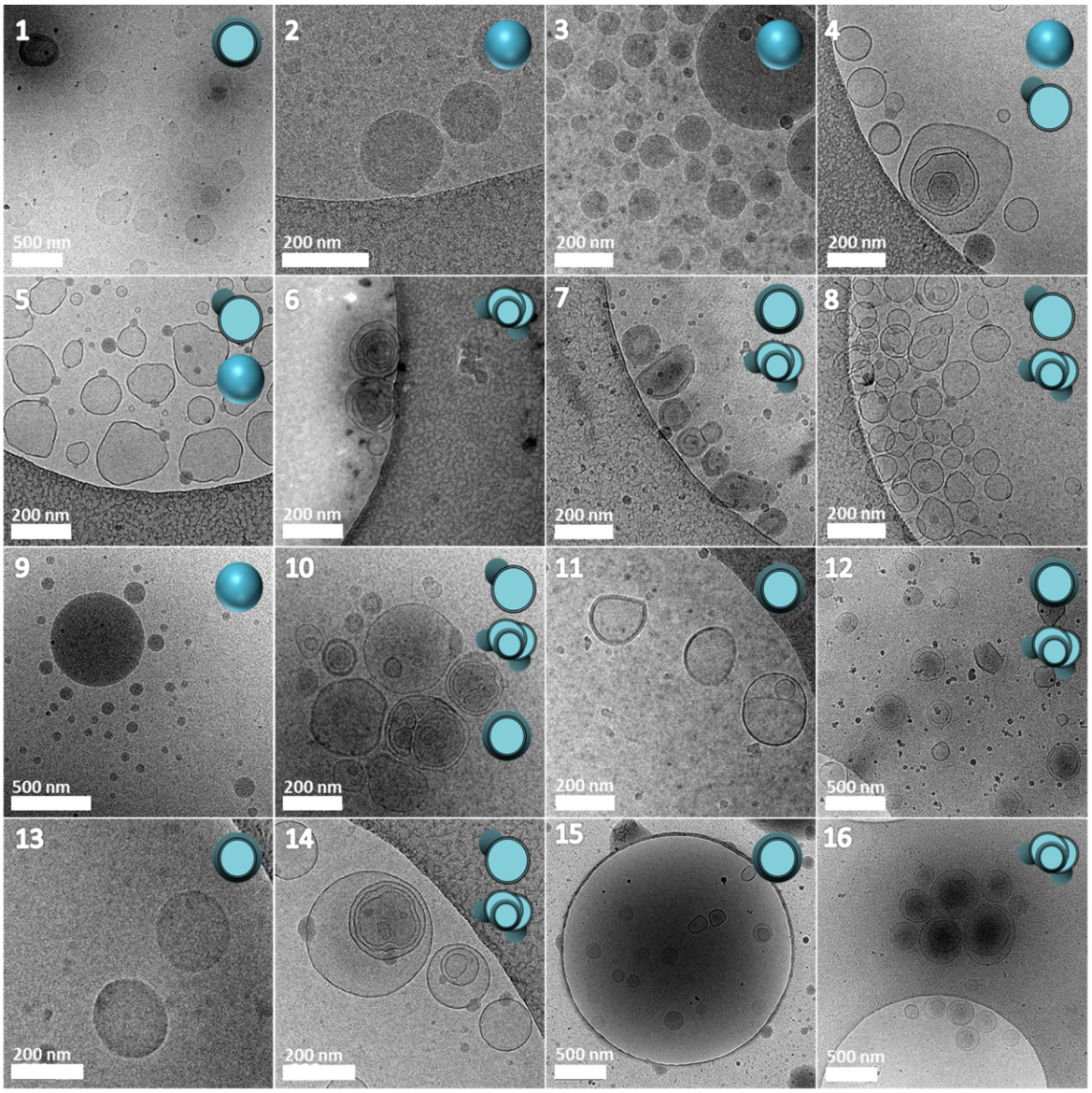

Figure 2. Cryo-TEM images of different types of precursor nanostructures prepared by random RAFT oligomers and DODAB vesicles from the experiments listed in Table 3.

Fraction of Multicompartment Structures. Multicompartment structures are the least frequently observed morphologies in this set of experiments. L and T were found to be the most important factors affecting the fraction of multicompartment structures, leading to

$$Y_m = 13.1 + 11.9\, L^1_{-1} + 6.9\, T^1_{-1} + 6.3\, L^1_{-1} \times T^1_{-1} \quad (2)$$

Although the predictive value of this equation is limited (r^2 = 61.1% and r_{adj}^2 = 51.4%), the equation and the data in Table 3 show that significant amounts of multicompartment structures are found for high values of L and the highest amounts for high L and high T.

Fraction of Capsules. The results in Table 3 already reveal at first glance that experiments with high levels of AA (high F_{AA}) result in higher fractions of spherical capsules than those with a low F_{AA}. This result is not that surprising when considering that the interaction between the deprotonated acrylic acid groups and the cationic charges of the vesicles are responsible for the adsorption of the oligomers onto the vesicles. The length L of the oligomers was also found to significantly affect the fraction of capsules as is clear from eq 3:

$$Y_c = 42.0 - 9.9\, L^1_{-1} + 33.9\, F_{AA^1_{-1}} - 10.0\, L^1_{-1} \times F_{AA^1_{-1}} \quad (3)$$

This dependence on L implies that the other monomer BA is also important. According to eq 3, with F_{AA} = 0.75 (+1 in coded units) and L = 18 (−1 in coded units), more than 85% of the product will be spherical capsules. With high F_{AA} and L, the fraction of capsules reduces to 55%, and (in the investigated parameter range) a minimum of Y_c = 8% is seen for long chains with low F_{AA} (i.e., for relative hydrophobic long oligomers). Under intermediate conditions ($F_{AA^1_{-1}}$ and L^1_{-1} are equal to zero), 42% capsules will be produced.

Fraction of Protrusion Structures. pH and F_{AA} were found to have the strongest influence on the occurrence of the protrusion structure. High pH and low F_{AA} result in more protrusion structures. Statistical analysis (see the Supporting Information) of the results leads to the following relationship:

DOI: 10.1021/acs.macromol.9b02182
Macromolecules 2019, 52, 9476−9483

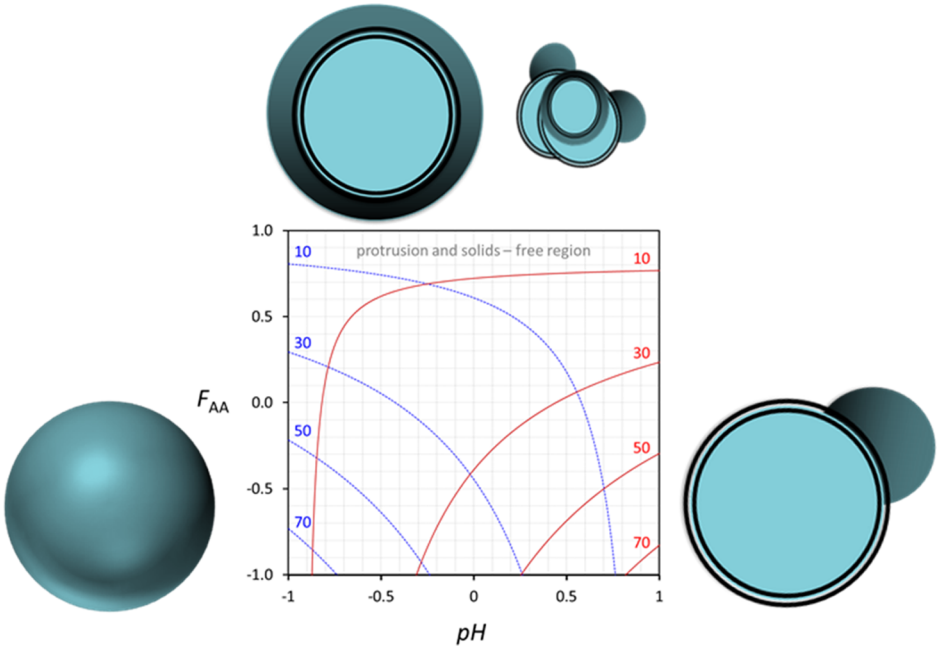

Figure 3. Contour plot of the protrusion structure (blue dashed lines) and solid spheres (red connected lines) based on eqs 4 and 5 estimating the percentage of each structure based on pH and F_{AA}. The schematic structures show the majority of morphologies observed on the corresponding side of the contour plot.

$$Y_p = 23.0 + 15.9\ pH^1_{-1} - 18.0\ F_{AA_{-1}}{}^1 - 19.6\ pH^1_{-1}F_{AA_{-1}}{}^1 \quad (4)$$

Within the range of investigated experimental conditions, a maximum amount of protrusion structures of Y_p = 77% is achieved at pH = 8 (+1 in coded units) and F_{AA} = 0.66 (−1 in coded units). So, for oligomers with a high BA content and all COOH deprotonated, this suggests the aggregation of BA segments.

Fraction of Solid Spheres. This study on RAFT-based encapsulation of vesicles is the first to report the occurrence of significant amounts of large solid spheres. In a few experiments of the current study, however, they constituted the dominant morphology. Experiments show that solid spheres mostly occur at low pH and low acrylic acid content in the system. Statistical analysis (see the Supporting Information) shows that the only significant factors that influence the fraction of solid spheres are the pH and fraction of AA in the oligomer, F_{AA} (see eq 2).

$$Y_s = 21.6 - 19.9\ pH^1_{-1} - 18.9F_{AA_{-1}}{}^1 + 20.1\ pH^1_{-1}F_{AA_{-1}}{}^1 \quad (5)$$

Effect of Oligomer Structure on Precursor Morphology. It is interesting now to consider the overall effect of the structure of the oligomer on the precursor morphology. Comparison of experiments 9 and 11 in Table 3 shows that changing from a low to a high F_{AA} (and T) changes the morphology from (nearly) all solid particles to nearly all capsules.[23,24] When we then compare these two experiments with experiments 2 and 4, which only differ by the fact that 9 and 11 involve short oligomers and 2 and 4 involve long oligomers, we see a very similar effect. Again, upon changing from a low to a high F_{AA} (and T), the morphology changes from nearly all solids to capsules, being the dominant morphology (61%). However, in the case of experiment 4, also, a significant fraction of multicompartment structures (19%) is formed. Hence, from these four experiments, we conclude that a high AA content in the oligomer is necessary for capsule formation (potentially in combination with a flexible bilayer (high T)), but that longer oligomer chain lengths convert the capsule structures to multicompartment structures.

Solid particles and protrusions (Y_s and Y_p) may also be connected, in the sense that a protrusion structure might disintegrate in a solid particle and residual vesicle material. Equation 6 suggests that the overall amount of solid and protrusion structures only depends on F_{AA}. The pH dependence of the occurrence of both structures is opposite, canceling out in the sum of the two structures.

$$Y_p + Y_s \approx 44 - 36F_{AA_{-1}}{}^1 \quad (6)$$

This equation is in line with our earlier statement that high F_{AA} leads to a reduction in solid particles (and results in more capsules). So, when we now consider the fraction of capsules that is produced at high F_{AA} (eq 7), we see indeed that this fraction only significantly affects the length of the oligomer.

$$Y_{c,\max F_{AA}} \approx 76 - 20L^1_{-1} \quad (7)$$

As stated before, this reduction in the fraction of capsules with large L (at high F_{AA}) leads to an increase in multicompartment structures.

A lower acrylic acid content (F_{AA}) automatically means a higher content of the more hydrophobic butyl acrylate, which in turn facilitates the formation of more compact and concentrated hydrophobic domains. In combination with a higher pH (and therefore more deprotonated AA groups), these domains are likely to be stabilized by negative charges and interact with the positive vesicle surface. The resulting structure would then be a protrusion structure as is schematically shown in Figure 3; as such, the protrusion structures can be considered as a hybrid structure combining a vesicle and a solid particle. Such a not fully covered vesicle with

DOI: 10.1021/acs.macromol.9b02182
Macromolecules 2019, 52, 9476−9483

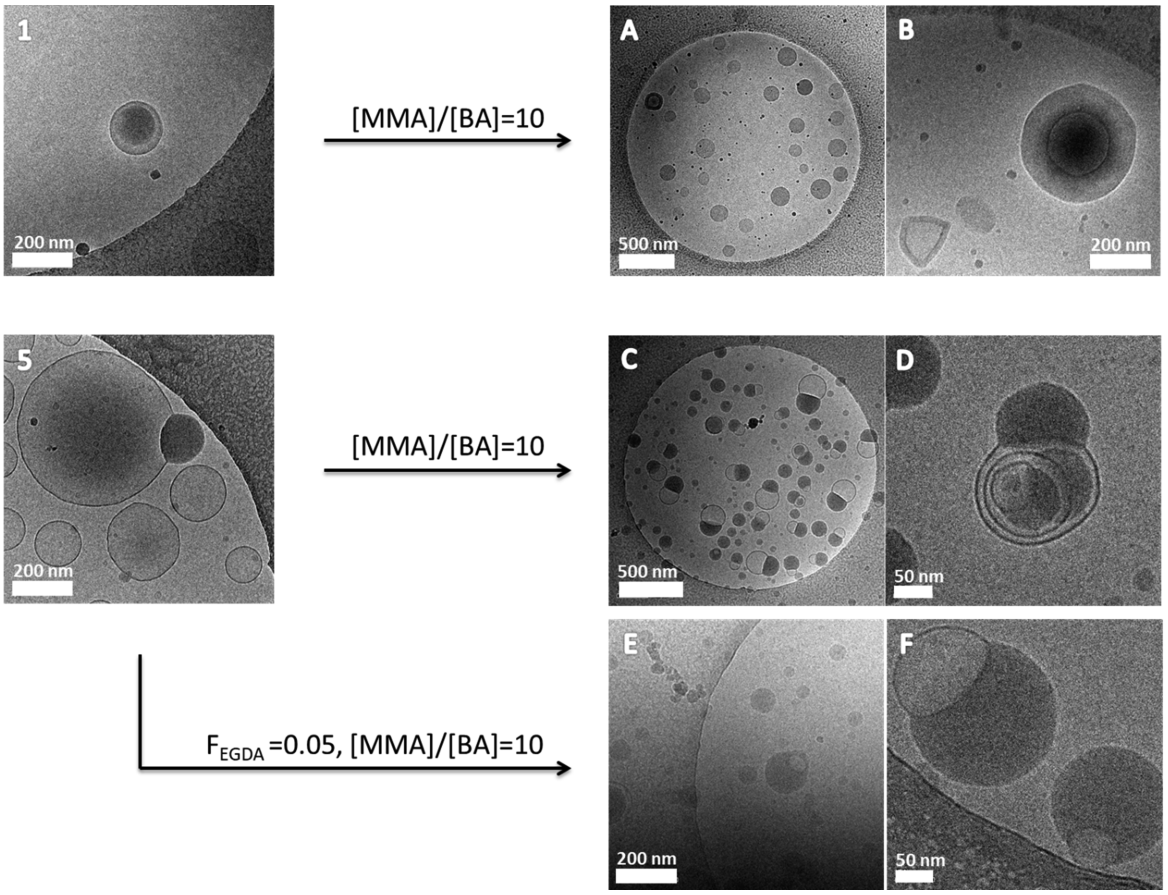

Figure 4. Polymerization of RAFT oligomer-vesicle templates with MMA/BA (10/1) monomer feed in starved feed emulsion polymerization: (A,B) nanocapsules growing from a circular template (C,D) polymerization from a protruded template, and (E,F) polymerization of a protruded template using 5% EGDA as the cross-linker.

a small polymer particle was previously called as parachute-like hybrid nanoparticle.[25]

An increase in the fraction of protrusion structures is indeed predicted by eq 4, which at the same time shows that a lowering of the pH results in a decrease in the fraction of protrusion structures. Since a lowering in pH leads to an increase in the fraction of solid particles (see eq 5), it is conceivable that a decrease in pH leads to a weaker interaction of the hydrophobic particles and the vesicles and that the particles simply do not attach. The question then would be why the typical vesicle structures seem to disappear. At this stage, we do not have a satisfying answer to this question other than that, under the low pH conditions, the vesicle structures may deform or integrate into the solid structures and become no longer visible.

Polymerization of Different RAFT Oligomer-Vesicle Precursors. Finally, we investigate the effect of the initial RAFT oligomer-vesicle precursor on the final morphology of the polymer nanostructure after chain extension. For these studies, we selected the precursors originating from experiments 1 (mainly capsules ~95%) and 5 (13% capsules and 87% protrusions) from Table 3. The RAFT oligomers in precursors 1 and 5 were both chain-extended by a monomer mixture of MMA and BA, and in addition, precursor 5 was also chain-extended with MMA/BA in the presence of the cross-linker EGDA. Representative cryo-TEM images of the dominant morphologies of the resulting polymer nanostructures are shown in Figure 4. It is clear from these images that the resulting polymer structures resemble those of the starting precursor, with the main additional morphology after polymerization being solid particles (see Table 4). In the case of precursor 1, it is not clear at this point whether these particles originate from a desorption of polymer particles from the vesicle surface (i.e., the protrusions) or whether they are the result of secondary nucleation. The results for precursor 5 suggest that the former process plays a role because the use of a cross-linker in the chain extension (E and F in Table 4) results in a much lower fraction of solids than in the absence of the cross-linker (C and D in Table 4); cross-linking seems to fix the protrusions to the polymer shell around the vesicle.

Table 4. Morphology Distribution of the Polymerized RAFT Oligomer-Vesicles Inferred from Figure 4

polymerization	solid (%)	capsule (%)	protrusion (%)	multicompartment (%)
A, B	23	70	6	1
C, D	58	4	33	5
E, F	28	10	62	0

When we now consider these results in the context of our previous work,[11] where under conditions of no added cross-linker still protrusion structures were observed in the structures after polymerization of the oligomer-vesicle precursor, it is interesting to predict the percentage of protrusions in the oligomer-vesicle precursors of that particular study. The conditions used in the previous study[11] are F_{AA} = 0.6 (close

DOI: 10.1021/acs.macromol.9b02182
Macromolecules 2019, 52, 9476−9483

to the lower limit of this study $F_{AA-1}^{1} \sim -1$), and pH = 7 (pH_{-1}^{1} = 0). Applying eq 4 leads to a rough estimate of Y_p = 41%. Hence, if the template is replicated into the final morphology after polymerization, indeed, a significant fraction of protrusions is expected in the product.

In conclusion, we can state that the final morphology of the resulting polymer nanostructure is to a very large extent determined by the morphology of the starting vesicle-RAFT oligomer precursor.

CONCLUSIONS

In this study, we have shown that the morphology of vesicle-RAFT oligomer precursors to polymer nanostructures can be controlled by variation in the oligomer structure and complexation conditions. We showed that high fractions of acrylic acid are required for obtaining capsules and multi-compartment structures, using short and long oligomers, respectively. Protruded capsules and solid particles are obtained using oligomers containing a low AA fraction. The results further suggest that these latter two morphologies as being related: protrusions are obtained at high pH, and solid particles are obtained at low pH, which suggests that the solid particles adsorb onto the vesicle surface when they contain more anionic AA groups. Finally, we have shown that the morphology of the polymer nanostructure after chain extension resembles that of the vesicle-RAFT oligomer precursor.

ASSOCIATED CONTENT

Supporting Information

The Supporting Information is available free of charge at https://pubs.acs.org/doi/10.1021/acs.macromol.9b02182.

Details for the characterization of compound stabity (DLS data), Pareto charts, and factorial regression of the DOE analysis (PDF)

AUTHOR INFORMATION

Corresponding Authors

*E-mail: m.a.moradi@tue.nl (M.-A.M.).
*E-mail: j.p.a.heuts@tue.nl (J.P.A.H.).

ORCID

Mohammad-Amin Moradi: 0000-0003-3754-9200
Alexander M. van Herk: 0000-0001-9398-5408
Johan P. A. Heuts: 0000-0002-9505-8242

Notes

The authors declare no competing financial interest.

ACKNOWLEDGMENTS

We gratefully acknowledge partial financial support from the Stichting Emulsion Polymerization. Electron microscopy was performed at the Center for Multiscale Electron Microscopy at Eindhoven University of Technology. Portions of information contained in this publication are printed with permission of Minitab, LLC. All such materials remain the exclusive property and copyright of Minitab, LLC. All rights reserved.

REFERENCES

(1) Huang, X.; Zhao, Y.; Ao, Z.; Wang, G. Micelle-Template Synthesis of Nitrogen-Doped Mesoporous Graphene as an Efficient Metal-Free Electrocatalyst for Hydrogen Production. *Sci. Rep.* **2014**, *4*, 7557.

(2) Deng, Y.; Wei, J.; Sun, Z.; Zhao, D. Large-Pore Ordered Mesoporous Materials Templated from Non-Pluronic Amphiphilic Block Copolymers. *Chem. Soc. Rev.* **2013**, *42*, 4054−4070.

(3) Valtchev, V.; Tosheva, L. Porous Nanosized Particles: Preparation, Properties, and Applications. *Chem. Rev.* **2013**, *113*, 6734−6760.

(4) Borges, J.; Rodrigues, L. C.; Reis, R. L.; Mano, J. F. Layer-by-Layer Assembly of Light-Responsive Polymeric Multilayer Systems. *Adv. Funct. Mater.* **2014**, *24*, 5624−5648.

(5) Cuomo, F.; Lopez, F.; Miguel, M. G.; Lindman, B. Vesicle-Templated Layer-by-Layer Assembly for the Production of Nanocapsules. *Langmuir* **2010**, *26*, 10555−10560.

(6) Shutava, T. G.; Pattekari, P. P.; Arapov, K. A.; Torchilin, V. P.; Lvov, Y. M. Architectural Layer-by-Layer Assembly of Drug Nanocapsules with PEGylated Polyelectrolytes. *Soft Matter* **2012**, *8*, 9418−9427.

(7) Ali, S. I.; Heuts, J. P. A.; van Herk, A. M. Vesicle-Templated PH-Responsive Polymeric Nanocapsules. *Soft Matter* **2011**, *7*, 5382.

(8) Ali, S. I.; Heuts, J. P. A.; van Herk, A. M. Controlled Synthesis of Polymeric Nanocapsules by RAFT-Based Vesicle Templating. *Langmuir* **2010**, *26*, 7848−7858.

(9) Loiko, O. P.; van Herk, A. M.; Ali, S. I.; Burkeev, M. Z.; Tazhbayev, Y. M.; Zhaparova, L. Z. Controlled Release of Capreomycin Sulfate from PH-Responsive Nanocapsules. *e-Polymers* **2013**, *13*, 189−202.

(10) Ali, S. I.; Heuts, J. P. A.; Hawkett, B. S.; van Herk, A. M. Polymer Encapsulated Gibbsite Nanoparticles: Efficient Preparation of Anisotropic Composite Latex Particles by RAFT-Based Starved Feed Emulsion Polymerization. *Langmuir* **2009**, *25*, 10523−10533.

(11) Moradi, M.-A.; Bomans, P. H. H.; Jackson, A. W.; van Herk, A. M.; Heuts, J. P. A. A Quantitative CryoTEM Study on Crosslinked Nanocapsule Morphology in RAFT-Based Vesicle Polymerization. *Eur. Polym. J.* **2018**, *108*, 329−336.

(12) Aguirre, G.; Ramos, J.; Heuts, J. P. A.; Forcada, J. Biocompatible and Thermo-Responsive Nanocapsule Synthesis through Vesicle Templating. *Polym. Chem.* **2014**, *5*, 4569−4579.

(13) Jung, M.; Hubert, D. H. W.; Bomans, P. H. H.; Frederik, P.; Van Herk, A. M.; German, A. L. A Topology Map for Novel Vesicle-Polymer Hybrid Architectures. *Adv. Mater.* **2000**, *12*, 210−213.

(14) Jung, M.; Hubert, D. H. W.; Bomans, P. H. H.; Frederik, P. M.; Meuldijk, J.; Van Herk, A. M.; Fischer, H.; German, A. L. New Vesicle-Polymer Hybrids: The Parachute Architecture. *Langmuir* **1997**, *13*, 6877−6880.

(15) Jung, M.; Hubert, D. H. W.; van Veldhoven, E.; Frederik, P.; van Herk, A. M.; German, A. L. Vesicle−Polymer Hybrid Architectures: A Full Account of the Parachute Architecture. *Langmuir* **2000**, *16*, 3165−3174.

(16) Dergunov, S. A.; Schaub, S. C.; Richter, A.; Pinkhassik, E. Time-Resolved Loading of Monomers into Bilayers with Different Curvature. *Langmuir* **2010**, *26*, 6276−6280.

(17) Montgomery, D. C. *Design and Analysis of Experiments*; 9th Ed.; John wiley & sons, 2017.

(18) Dergunov, S. A.; Kesterson, K.; Li, W.; Wang, Z.; Pinkhassik, E. Synthesis, Characterization, and Long-Term Stability of Hollow Polymer Nanocapsules with Nanometer-Thin Walls. *Macromolecules* **2010**, *43*, 7785−7792.

(19) Meier, W. Polymer Nanocapsules. *Chem. Soc. Rev.* **2000**, *29*, 295−303.

(20) Lim, H. J.; Cho, E. C.; Shim, J.; Kim, D.-H.; An, E. J.; Kim, J. Polymer-Associated Liposomes as a Novel Delivery System for Cyclodextrin-Bound Drugs. *J. Colloid Interface Sci.* **2008**, *320*, 460−468.

(21) Antunes, F. E.; Marques, E. F.; Miguel, M. G.; Lindman, B. Polymer-Vesicle Association. *Adv. Colloid Interface Sci.* **2009**, *147-148*, 18−35.

(22) *Minitab 17 Statistical Software (2010)*. [Computer software]. State College, PA: Minitab, Inc. www.minitab.com.

(23) Scarioti, G. D.; Lubambo, A.; Feitosa, J. P. A.; Sierakowski, M. R.; Bresolin, T. M. B.; de Freitas, R. A. Nanocapsule of Cationic

DOI: 10.1021/acs.macromol.9b02182
Macromolecules 2019, 52, 9476−9483

Liposomes Obtained Using "in Situ" Acrylic Acid Polymerization: Stability, Surface Charge and Biocompatibility. *Colloids Surf., B* **2011**, *87*, 267−272.
(24) Bazzano, M.; Pisano, R.; Brelstaff, J.; Spillantini, M. G.; Sidoryk-Wegrzynowicz, M.; Rizza, G.; Sangermano, M. Synthesis of Polymeric Nanocapsules by Radical UV-Activated Interface-Emulsion Polymerization. *J. Polym. Sci., Part A: Polym. Chem.* **2016**, *54*, 3357−3369.
(25) Jung, M.; Hubert, D. H. W.; van Veldhoven, E.; Frederik, P. M.; Blandamer, M. J.; Briggs, B.; Visser, A. J. W. G.; van Herk, A. M.; German, A. L. Interaction of Styrene with DODAB Bilayer Vesicles. Influence on Vesicle Morphology and Bilayer Properties. *Langmuir* **2000**, *16*, 968−979.

DOI: 10.1021/acs.macromol.9b02182
Macromolecules 2019, 52, 9476−9483